

# X-ray microtomography as a new approach for imaging and analysis of tumor spheroids

Hanieh Karimi<sup>a,1</sup>, Bartosz Leszczyński<sup>a,\*,1</sup>, Tomasz Kołodziej<sup>b</sup>, Ewelina Kubicz<sup>c</sup>,  
Małgorzata Przybyło<sup>d</sup>, Ewa Stępień<sup>a</sup>

<sup>a</sup> Department of Medical Physics, M. Smoluchowski Institute of Physics, Faculty of Physics, Astronomy and Applied Computer Science, Jagiellonian University, Kraków, Poland

<sup>b</sup> Department of Molecular and Interfacial Biophysics, M. Smoluchowski Institute of Physics, Faculty of Physics, Astronomy and Applied Computer Science, Jagiellonian University, Kraków, Poland

<sup>c</sup> Department of Experimental Particle Physics and Applications, M. Smoluchowski Institute of Physics, Faculty of Physics, Astronomy and Applied Computer Science, Jagiellonian University, Kraków, Poland

<sup>d</sup> Department of Glycoconjugate Biochemistry, Institute of Zoology and Biomedical Research, Faculty of Biology, Jagiellonian University, Kraków, Poland

## ARTICLE INFO

### Keywords:

Spheroids  
Cellular  
Micro-CT  
Melanoma  
Microscopy  
Cell line  
Cell culture techniques

## ABSTRACT

Three-dimensional (3D) spheroids mimic important properties of tumors and may soon become a reasonable substitute for animal models and human tissue, eliminating numerous problems related to *in vivo* and *ex vivo* experiments and pre-clinical drug trials. Currently, various imaging methods including X-ray microtomography (micro-CT), exist but their spatial resolution is limited. Here, we visualized and provided a morphological analysis of spheroid cell cultures using micro-CT and compared it to that of confocal microscopy. An approach is proposed that can potentially open new diagnostic opportunities to determine the morphology of cancer cells cultured in 3D structures instead of using actual tumors.

Spheroids were formed from human melanoma cell lines WM266-4 and WM115 seeded at different cell densities using the hanging drop method. Micro-CT analysis of spheroid showed that spheroid size and shape differed depending on the cell line, initial cell number, and duration of culture.

The melanoma cell lines used in this study can successfully be cultured as 3D spheroids and used to substitute human and animal models in pre-clinical studies. The micro-CT allows for high-resolution visualization of the spheroids structure.

## 1. Introduction

Melanoma is the most dangerous type of skin cancer and remains the main cause of skin cancer-related deaths even though it is responsible for only about 1% of all skin cancer cases (Society, 2018). Melanoma is a multifactorial disease in which both genetic susceptibility and environmental exposure, predominantly to ultraviolet light, play important roles (Wróbel et al., 2019). The incidence of melanoma is rapidly increasing with approximately 350,000 new cases reported worldwide each year (Karimkhani et al., 2017). As the effectiveness of melanoma treatment at advanced stages is low, there is a constant need for the development of new, targeted therapies, immunotherapy, and combination therapies.

For decades, animal models and 2D *in vitro* cultures have been the standard approaches for determining the effects that biological molecules and therapeutic drugs have on different types of diseases, including cancer. Over the past two decades, however, several new methods such as nanobiosensors, multicellular 3D spheroids, and radioactive carries have been developed to evaluate and treat different types of cancers (Stępień et al., 2020). One of the most promising pre-clinical *in vitro* methods is 3D spheroids as they can mimic the structure of tumors under physiological conditions. The morphology and cell-cell interactions in 3D spheroids are completely different from monolayer cell culture. Tumor 3D spheroids hold certain advantages over standard research methods, including low cost of use, high reproducibility and time-saving, and reduces the need for laboratory animal models (Costa

\* Corresponding author.

E-mail addresses: [hanieh.karimi@doctoral.uj.edu.pl](mailto:hanieh.karimi@doctoral.uj.edu.pl) (H. Karimi), [bartosz.leszczyński@uj.edu.pl](mailto:bartosz.leszczyński@uj.edu.pl) (B. Leszczyński), [tomasz.kolodziej@doctoral.uj.edu.pl](mailto:tomasz.kolodziej@doctoral.uj.edu.pl) (T. Kołodziej), [ewelina.kubicz@doctoral.uj.edu.pl](mailto:ewelina.kubicz@doctoral.uj.edu.pl) (E. Kubicz), [malgorzata.przybylo@uj.edu.pl](mailto:malgorzata.przybylo@uj.edu.pl) (M. Przybyło), [e.stepien@uj.edu.pl](mailto:e.stepien@uj.edu.pl) (E. Stępień).

<sup>1</sup> Equally contributed to the manuscript.

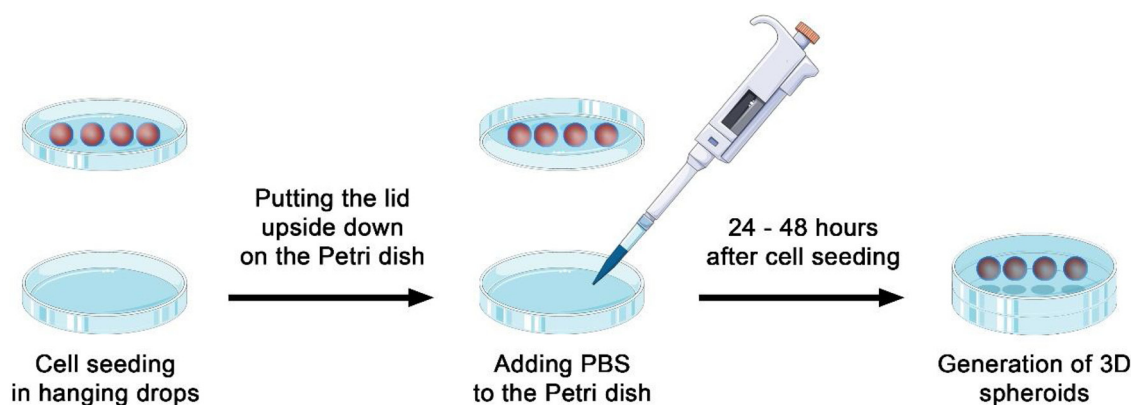


Fig. 1. A graphical illustration of the formation of three-dimensional (3D) spheroids in Petri dishes using a hanging drop method.

et al., 2016; Pampaloni et al., 2013). The unique properties of 3D tumor spheroids make them invaluable for biological experiments and drug tests in a variety of experimental studies focused on chemotherapy and radiotherapy (Hirschhaeuser et al., 2010).

A typical spheroid is a three-layered structure and each cell layer has a different proliferation rate, reminiscent of solid tumors, especially in terms of internal and external structure, proliferation, and gene expression (Costa et al., 2016; Milotti et al., 2012, 2014). The deepest layer forms a core of necrotic cells, the middle layer contains quiescent cells, and the external layer is composed of proliferating cells. The specificity of layers is explained by the disparate access to oxygen and nutrients as well as the removal of metabolic waste due to different diffusion rates within specific layers (Costa et al., 2016; Milotti et al., 2012, 2014). The proliferation rate of spheroids varies at different developmental stages just as observed in solid tumors. Several methods can be used to produce 3D spheroids such as liquid overlay, hanging drop, rotary vessel bioreactors, and spinner flask methods (Raghavan et al., 2015; Shi et al., 2018). Compared to other methods, the hanging drop cell culture is the most common as it does not require any special equipment, and is easy to perform (Müller and Kulms, 2018).

X-ray microtomography (micro-CT) is a nondestructive method that provides spatial resolution at the micron level and is well-suited for the visualization of internal structures and the analysis of small samples. Over the last decade, micro-CT has become a gold standard in pre-clinical imaging and has been particularly useful in the pre-clinical investigation of calcified tissues such as bones and teeth (Bouxsein et al., 2010; Rosenhain et al., 2018). These tissues contain elements with high atomic numbers which attenuate X-rays very well, thereby producing good image contrast. Conversely, differences in X-ray attenuation between soft tissues are minimal and the overall attenuation effect is similar to that observed for water, creating a very weak contrast of soft tissue images. However, the image quality can be significantly improved using several staining methods. Although the idea of staining originated from histological studies, micro-CT requires a lot more of the staining solution because of high sample volumes. The success of micro-CT visualization depends on molecular diffusion of contrast agent into the tissue. The staining time is also longer and can even take up to weeks for large samples. The most common staining protocols used are Lugol solution ( $I_2/KI$ ), osmium tetroxide ( $OsO_4$ ), or phosphotungstic acid (PTA) (Metscher, 2009; Leszczyński et al., 2018).

In the present study, the ability of two human melanoma cell lines WM266-4 and WM115 to form 3D spheroids was compared and micro-CT was used as a new approach to studying spheroid morphology.

## 2. Material and methods

### 2.1. Cell culture

Two cutaneous melanoma cell lines were obtained from the ESTDAB

Melanoma Cell Bank (Tübingen, Germany). The WM115 (primary) and WM266-4 (metastatic) cell lines originated from the same individual and represented radial/vertical growth phase and lymph node metastasis, respectively (Herlyn et al., 1985). These cells were cultured in non-treated cell culture flasks (GenoPlast, Biochemicals, cat. no 708011, Rokocin, Poland) and maintained in an incubator at 37 °C and 5%  $CO_2$  with humidity. Both cell lines were cultured in complete culture media, which consisted of RPMI 1640 (Gibco, cat. no 21875091, Waltham, MA USA) supplemented with 10 % fetal bovine serum (FBS) (Gibco, cat. no 10500064, Waltham, MA USA) and 1% penicillin-streptomycin (Gibco, cat. no 15140122, Waltham, MA USA). Cells from passage 19–23 with the number of living cells higher than 90 % in total cells were used to generate spheroids. A trypan blue assay with a Luna-II TM automated cell counter was used to perform cell counts and a viability test prior to seeding cells.

### 2.2. Formation of melanoma spheroids

Each cell line was seeded at a different cell density (500, 1000, or 1500 cells) in drops of 15  $\mu$ L of RPMI. Drops were formed on the lids of 6 mL Petri dishes and the culture medium of each drop was changed every 48 h. The bottom of each Petri dish was filled with 5 mL of PBS (Gibco, cat. no 10010056, Waltham, MA USA) to prevent drops from drying out and to provide humidity (Fig. 1). Petri dishes were subsequently placed in an incubator and maintained under standard cell culture conditions to allow for spheroid formation. Spheroids were formed after 24–48 h of incubation depending on the cell line. The morphology and growth of spheroids were assessed after 2, 5, and 7 days of spheroid growth. Spheroid structure was determined by optical microscopy (Olympus, IX-LWPO, T2, Japan).

### 2.3. Proliferation and evaluation of cell viability

Cell viability during spheroid formation was determined using standard fluorescence dyes: propidium iodide (PI) (SIGMA, cat. no P-4170), fluorescein diacetate (FDA) (SIGMA, cat. no F-7378), and calcein staining (Thermo Fisher Scientific, cat. no C1430). To evaluate the rate of living cells in WM266-4 spheroids, FDA (5 mg/mL) and calcein (1 mg/mL) was used, while PI (0.4 mg/mL) was used to evaluate the rate of dead cells. To stain spheroids, a single spheroid was transferred to a glass-bottom dish and 100  $\mu$ L of staining solution was added. The stained spheroid was subsequently incubated at 37 °C for 10 min and gently washed twice with PBS (Fig. 2). Thereafter, 100  $\mu$ L of complete culture media was added to the spheroid before observation under an epifluorescence microscope. Since FDA and calcein can cross the membrane of living cells, whereas PI can only enter dead cells, cells that fluoresced green were considered viable, while cells with red fluorescence were considered non-viable. The percentage of death cells has been calculated as a percentage of red fluorescence area. This staining

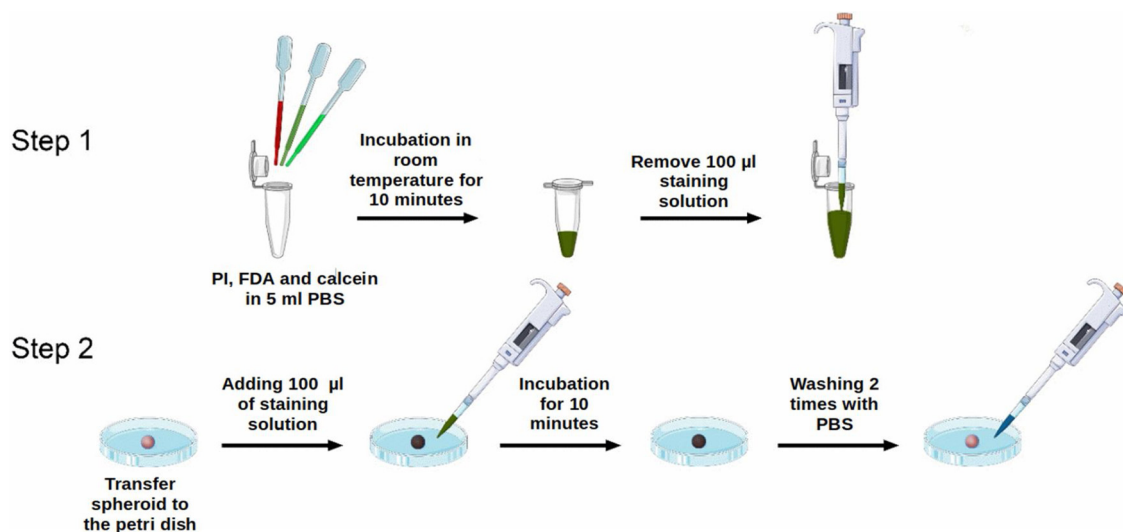


**Fig. 2.** A schematic representation of the fluorescence microscopy staining protocol. Step 1: Preparation of the fluorescence staining solution. Step 2: Staining of a single spheroid.

allowed for the evaluation of the spatial distribution of dead and living cells in spheroids.

#### 2.4. Micro-CT protocol and image processing

Micro-CT analysis was carried out with a Bruker SkyScan 1172 scanner (Bruker microCT, Kontich, Belgium) and scanning parameters were set to 40 keV without physical filtration. Images were captured with a spatial resolution of 1–2  $\mu\text{m}$  per pixel. To enhance the signal-to-noise ratio, each projection image was taken as the average of 10 frames.

Optimization of micro-CT staining included samples that were not fixed and samples that were fixed with 4% formaldehyde for 15 min. Standard micro-CT staining solutions, Lugol solution (SIGMA, cat. no 62,650) and 10 % PTA (SIGMA, cat. no P4006), were used and the incubation period for staining was experimentally optimized for between 30 min and 24 h. After staining, samples were washed with PBS and scanned (Fig. 3). Captured data was reconstructed and processed with Bruker software (Bruker microCT, Kontich, Belgium) Nrecon (v. 1.7.3.1) and CTAnalyzer (v. 1.18.8.0+), respectively. An anisotropic diffusion filter was applied to reduce image noise and images were binarized by histogram-based global thresholding. Afterwards, the 3D watershed separation algorithm was used to separate individual clusters of the spheroid.

#### 2.5. Data analysis

Spheroid growth rate was analyzed with ImageJ (v 1.52n) software according to the morphological parameters circular equivalent diameter, circularity, and roundness. Appropriate optical microscopy images were selected to perform this analysis for both melanoma cell lines (Fig. 4a, b). Spheroids were manually isolated as individual regions of interest (ROIs) and the above-mentioned morphological parameters were calculated after 2, 5 and 7 days of spheroid growth. The ImageJ software was also used to calculate the percentage of dead cell area as the red color area in the whole spheroid in fluorescence images (Fig. 5).

### 3. Results

#### 3.1. Size of spheroids

The size of spheroids significantly increased along with the length of

the culture. Spheroid size depended on the number of cells seeded at the start of culture. In general, WM115 spheroids exhibited an rapid growth rate (Fig. 4c). After 48 h, WM115 spheroids formed from 500 cells grew to a diameter of 310  $\mu\text{m}$  and reached a diameter of 470  $\mu\text{m}$  in one week, exhibiting a growth rate of 32  $\mu\text{m}/\text{day}$ . WM115 spheroids formed from 1000 cells grew to a diameter of 360  $\mu\text{m}$  after 48 h and reached 470  $\mu\text{m}$  in diameter after one week, exhibiting a growth rate of 22  $\mu\text{m}/\text{day}$ . In 48 h, WM115 spheroids formed from 1500 cells grew to a diameter of 390  $\mu\text{m}$  and, after one week, grew to 480  $\mu\text{m}$  in diameter, exhibiting a growth rate of 18  $\mu\text{m}/\text{day}$ .

Overall, WM266-4 spheroids demonstrated a stable growth rate (Fig. 4d). The growth rate of WM266-4 spheroids seeded at 500 cells was the highest and grew 10  $\mu\text{m}/\text{day}$ , while spheroids seeded at 1500 cells grew at 9  $\mu\text{m}/\text{day}$ . The lowest growth rate observed was of WM266-4 spheroids seeded at 1000 cells, which grew at 8  $\mu\text{m}/\text{day}$ . WM266-4 spheroids formed from 500 cells had a diameter of 380  $\mu\text{m}$  after 48 h and grew to 430  $\mu\text{m}$  in diameter after one week. WM266-4 spheroids formed from 1000 cells reached a diameter of 430  $\mu\text{m}$  after 48 h and reached a diameter of 470  $\mu\text{m}$  after one week. WM266-4 spheroids formed from 1500 cells grew to a diameter of 480  $\mu\text{m}$  after 48 h and reached 525  $\mu\text{m}$  in diameter after one week.

As the number of seeded cells increased, the growth rate concomitantly decreased likely due to the competition for oxygen and nutrients, especially in the case of WM115 spheroids. The growth rate also gradually decreased as the length of culturing increased. This is particularly evident in spheroids seeded at higher cell densities and could be attributed to a lack of sufficient nutrition and oxygen due to competition (compare in Fig. 4).

#### 3.2. Shape analysis

Over the course of one week, WM266-4 spheroids showed a clear increase in both circularity and roundness for all initial cell densities (Fig. 4g, h). This means that spheroids became rounder and more symmetric with a smoother surface. The WM115 spheroids, however, did not demonstrate such a clear correlation between circularity or roundness and time (Fig. 4d, e).

#### 3.3. Spheroid characteristics

The growth rate of spheroids formed by both melanoma cell lines showed continuous growth over the course of one week. The viability of cells in the different zones of a single spheroid was evaluated 5 and 7

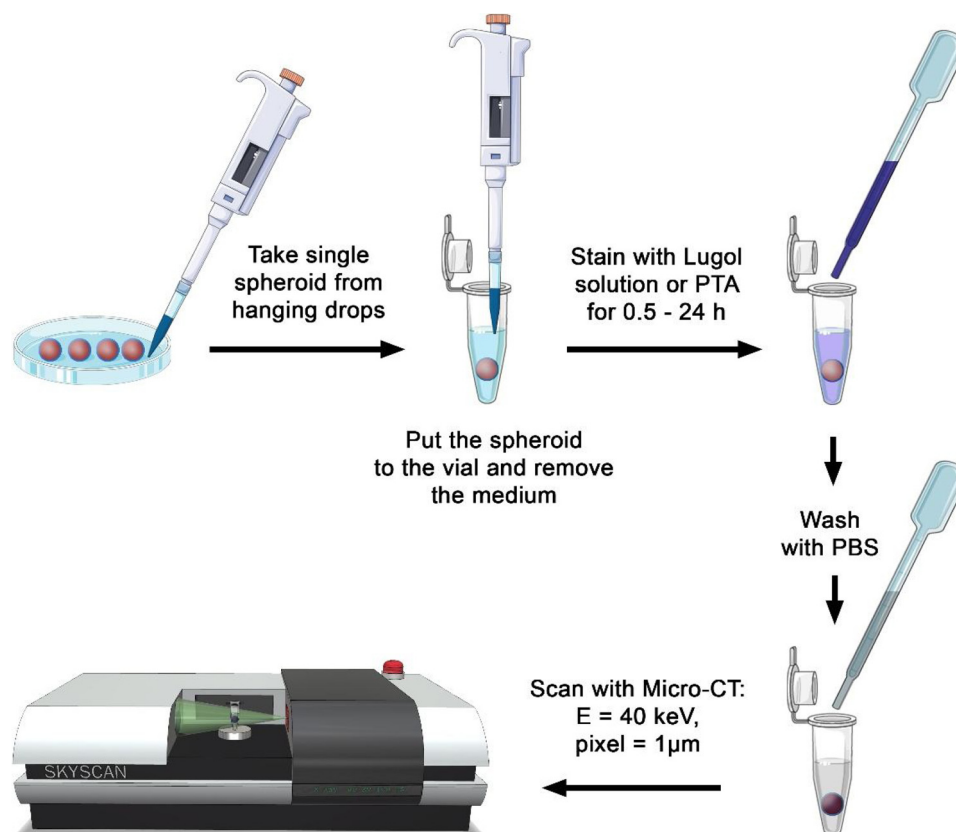


Fig. 3. A schematic representation of the micro-CT process.

days after seeding. The viability of spheroids were classified by fluorescence microscopy: green fluorescence indicated viable cells and red indicated dead cells. Viable cells were found mostly on the surface and the edge of the spheroid, whereas dead cells were located predominantly in the center of the spheroid. Interestingly, inside the spheroids different internal layers did not exhibit fluorescence and some contained a small number of dead cells. Furthermore, with the progression of time the red core increased in size from 0% to about 29 % of dead cell area, demonstrating how the spheroid grew and that cells in the central zone gradually died due to lack of oxygen and nutrients (Fig. 5).

### 3.4. Micro-CT

Optimization of micro-CT procedure proved challenging as the results were highly variable, demonstrating sensitivity to even subtle changes in the contrasting and fixation protocols. The spheroids were found to be highly sensitive to some of the staining and/or fixation methods used, which can cause deformation or even death of the spheroids. The most suitable image was obtained after staining for 1.5 h with Lugol solution, without fixation. After applying a combination of image denoising and Otsu thresholding it was possible to perform a 3D watershed separation to analyze individual spheroid and final visualizations of spheroids were obtained using volume rendering in CTVox software (v. 3.3.0 r.1403, Bruker micro-CT, Kontich, Belgium) (Fig. 6). More detailed explanation about a scale translation is available in Suppl 1. Spheroids from both cell lines grew and, over time, developed into more dense structures. However, WM266-4 cells produced a single, well-defined spheroid with a smooth surface (Fig. 6c, d), while WM115 cells were scattered and produced clusters of low-diameter spheroids instead (Fig. 6a, b). Technical details about Fig. 6 are described in the supplementary (Suppl 1).

## 4. Discussion

Over the past decade, many efforts have been made to improve drug tests and therapeutic methods. One of the new approaches in the field of tumor and chemotherapy research is the use of 3D spheroids which can potentially be a good replacement for using animal models and patient tissues because of their 3D architecture and establishment of cell-cell contacts (Torisawa et al., 2007). An important aspect of medical and pharmacology studies is the need to comply with ethical guidelines and regulations. However, working with 3D spheroids established from cell lines can eliminate these and other limitations. 3D spheroids are spherical cellular aggregates in which the cells are in close contact with each other, mimicking *in vivo* conditions. Because of this similarity, spheroids can be used reliably to determine gene expression and cell biological characteristics (Torisawa et al., 2007; Koide et al., 1990).

Since tumors start as a low density of cells, which then grow and proliferate, studies investigating the behavior of low cell densities in response to chemical and pharmaceutical stimulation can use spheroids as a convenient model to find more precise and reliable diagnostic and therapeutic approaches. In this study, spheroids were cultured at different cell densities and their growth rate and size was assessed over the period of culture. Studies conducted on 3D cell culture enable us to control the size and volume of spheroids as a tumor model, as well as evaluate cancer cell behavior at different stages and under different conditions, which reflects their behavior of the real tumor.

In our study, we noticed that necrotic area increased with time of culturing. That necrosis was more significant in bigger spheroids with one exception for 7 day old spheroid from WM266-4 cell line with 1500 initial cells. This discrepancy was probably due to reaching the maximum size of the necrotic core (Fig. 5b). We observed cells which were neither green (alive) or red (dying) in fluorescence (Fig. 5). There are at least two explanations of this phenomenon: (1) fluorescence

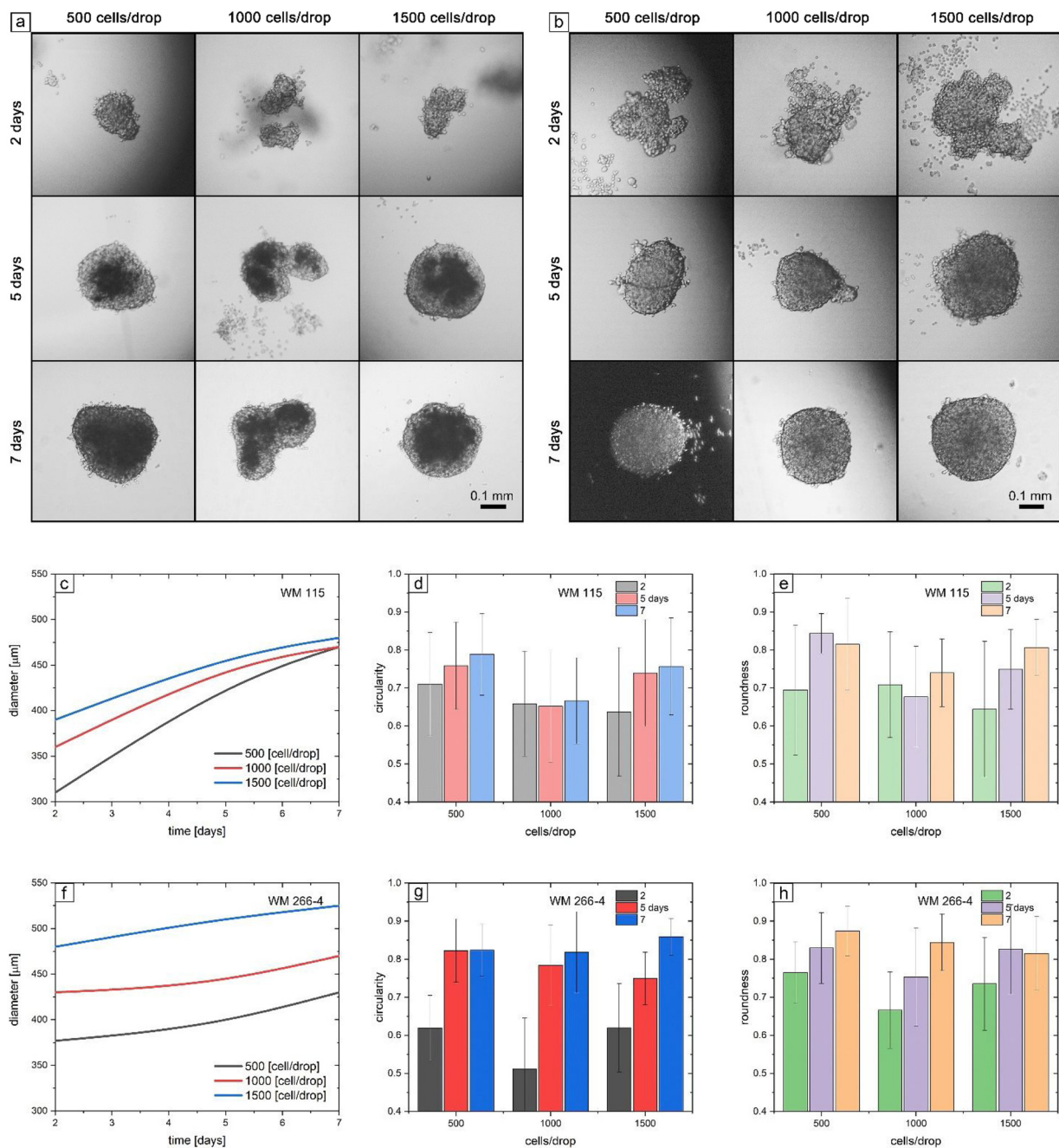


**Fig. 4.** Optical microscopy images of melanoma cell lines WM115 (a), WM266-4 (b). The growth rate, circularity, and roundness of spheroids formed by melanoma cell lines WM115 (c-e) and WM266-4 (f-h), respectively.

attenuation by melanin/eumelanin and (2) poor fluorescent dye diffusion. Firstly, melanoma cells are originated from melanocytes - neural-crest derived cells that contain a black pigment (melanin) or a red pigment (eumelanin). EPR (electron paramagnetic resonance) spectroscopy confirmed (data not shown) that both (WM266-4 and WM115) cell lines have eumelanin and pheomelanin pigment which can absorb light in the spectra by calcein and fluorescein emission: 515 and 525 nm, respectively (Nofsinger et al., 1999). Secondly, calcein and fluorescein diacetate are water soluble dyes and their diffuse is limited to solvent penetration. Moreover, fluorescein emission signal is quenching on conjugation to biopolymers and it is sensitive to pH changes: the strongest signal is observed at base pH (9.0) and the lowest at acidic conditions (5.0), which is expected in the inner compartments (Doughty, 2010).

Usually, common fluorescent microscopy techniques are sufficient

for most of experiments using spheroids as a model, especially those from a single cell line. Currently, other methods have been applied to bring more insight about multicellular spheroid structure e. g. optical coherence tomography (OCT), as refractive index (RI) has the potential to be used as a marker for spheroid growth phase (Hari et al., 2019).

Micro-CT has already been successfully used for imaging animal tissues and biological samples but, in this study, we showed that micro-CT can also be used to visualize and analyze spheroids in 3D. In contrast to microscopy methods, micro-CT allows for the reconstruction of the shape, surface, and internal structure of the spheroids in 3D. We hope that similarly to OCT, micro-CT will become a complimentary method for spheroid imaging.

Spheroids are very sensitive to the fixative and staining solutions and the best results were obtained after staining for 90 min with Lugol solution without fixation. In this study, the comparisons between

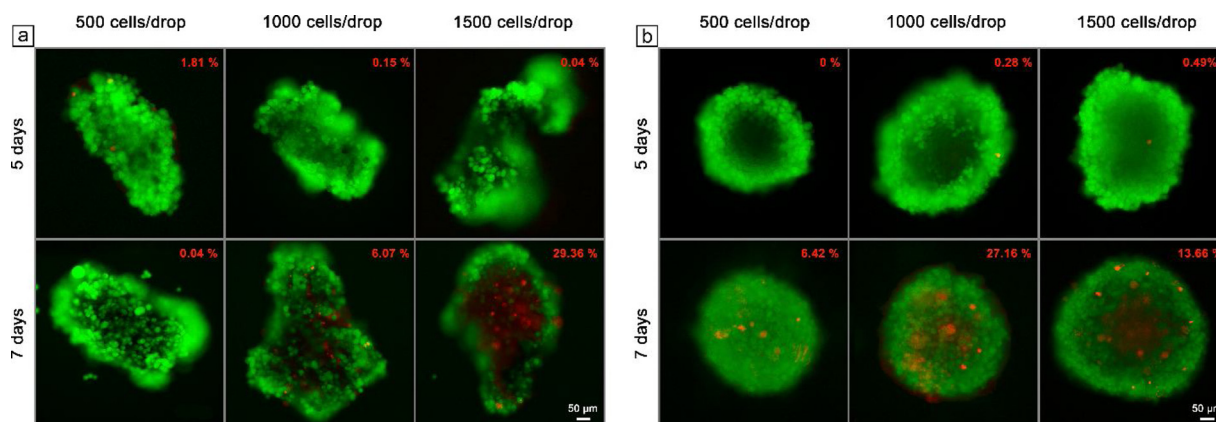


Fig. 5. Fluorescence images of WM115 (a) and WM266-4 (b) spheroids taken 5 and 7 days after seeding. In the top-right corner there is a death (red) cells percentage. (For interpretation of the references to colour in this figure legend, the reader is referred to the web version of this article).

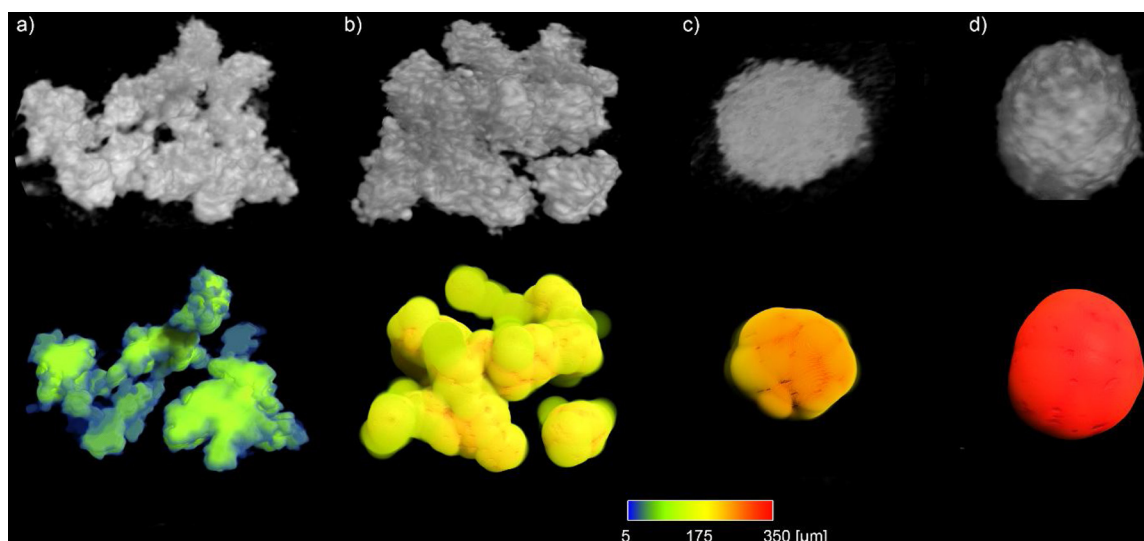


Fig. 6. Three-dimensional (3D) micro-CT models of spheroids formed by WM115 cells after 5 days (a), 7 days (b) and WM266-4 cells after 5 days (c), 7 days (d). Scale indicates the diameter of formed spheroids (Suppl 1).

confocal and micro-CT model were not fully displayed, especially in terms of necrotic zone determination. For the more adequate necrotic core visualization, the more adequate contracting agent should be used. Presently, there is no such agent for necrotic cell visualization and there is a need for developing such a lipid-specific contrasting agent. Micro-CT is capable to visualize any type of spheroid, including mixed-cell, but such visualizations still has not been performed. Mixed-cell spheroids, mimic major features of *in vivo* tumors, especially cell-to-cell interactions and can model tumor environments (Khawar et al., 2018). Tissue differentiation and angiogenesis, for example in cardiac (Pitaktong et al., 2020) or cancer spheroids (Shah et al., 2019) can be visualized by means of micro-CT technique, and this approach would be helpful to observe vessel formation and structure. Moreover, multiple object analysis is possible and very convenient. It speeds up the workflow.

Concluding, micro-CT is a complimentary method for common optical technique to visualize spheroid morphology, however the staining protocol still needs to be optimized to avoid spheroid destruction and new contrasting agents dedicated to visualize a necrotic zone are needed.

#### Declaration of Competing Interest

The authors declare that there are no conflicts of interest.

#### Acknowledgments

We would like to express our particular gratitude to Professor Paweł Moskal for his professional guidance and valuable financial support by TEAM/2017-4/39 program and also our grateful thanks to Professor Mariusz Kepczyński for his great assistance in fluorescence images preparation and useful recommendations. This project was also supported by DSC grant, number N17/MNS/000023 funded by Jagiellonian University which was awarded to Mrs. Hanieh Karimi for her PhD research.

#### Appendix A. Supplementary data

Supplementary material related to this article can be found, in the online version, at doi:<https://doi.org/10.1016/j.micron.2020.102917>.

#### References

- Bouxsein, M.L., Boyd, S.K., Christiansen, B.A., Guldberg, R.E., Jepsen, K.J., Müller, R., 2010. Guidelines for assessment of bone microstructure in rodents using micro-computed tomography. *J. Bone Miner. Res.* 25, 1468–1486. <https://doi.org/10.1002/jbmr.141>.
- Costa, E.C., Moreira, A.F., de Melo-Diogo, D., Gaspar, V.M., Carvalho, M.P., Correia, I.J., 2016. 3D tumor spheroids: an overview on the tools and techniques used for their analysis. *Biotechnol. Adv.* 34, 1427–1441. <https://doi.org/10.1016/j.biotechadv.2016.11.002>.

- Doughty, M.J., 2010. PH dependent spectral properties of sodium fluorescein ophthalmic solutions revisited. *Ophthalm. Physiol. Opt.* 30, 167–174. <https://doi.org/10.1111/j.1475-1313.2009.00703.x>.
- Hari, N., Patel, P., Ross, J., Hicks, K., Vanholsbeeck, F., 2019. Optical coherence tomography complements confocal microscopy for investigation of multicellular tumour spheroids. *Sci. Rep.* 9, 10601. <https://doi.org/10.1038/s41598-019-47000-2>.
- Herlyn, M., Balaban, G., Benniselli, J., Guerry, I.V.D., Halaban, R., Herlyn, D., Elder, D.E., Maul, G.G., Steplewski, Z., Nowell, P.C., Clark, W.H., Koprowski, H., 1985. Primary melanoma cells of the vertical growth phase: similarities to metastatic Cells2. *JNCI J. Natl. Cancer Inst.* 74, 283–289. <https://doi.org/10.1093/jnci/74.2.283>.
- Hirschhaeuser, F., Menne, H., Dittfeld, C., West, J., Mueller-Klieser, W., Kunz-Schughart, L.A., 2010. Multicellular tumor spheroids: an underestimated tool is catching up again. *J. Biotechnol.* 148, 3–15. <https://doi.org/10.1016/j.jbiotec.2010.01.012>.
- Karimkhani, C., Green, A.C., Nijsten, T., Weinstock, M.A., Dellavalle, R.P., Naghavi, M., Fitzmaurice, C., 2017. The global burden of melanoma: results from the Global Burden of Disease Study 2015. *Br. J. Dermatol.* 177, 134–140. <https://doi.org/10.1111/bjd.15510>.
- Khawar, I.A., Park, J.K., Jung, E.S., Lee, M.A., Chang, S., Kuh, H., 2018. Three dimensional mixed-cell spheroids mimic stroma-mediated chemoresistance and invasive migration in hepatocellular carcinoma. *Neoplasia* 20, 800–812. <https://doi.org/10.1016/j.neo.2018.05.008>.
- Koide, N., Sakaguchi, K., Koide, Y., Asano, K., Kawaguchi, M., Matsushima, H., Takenami, T., Shinji, T., Mori, M., Tsuji, T., 1990. Formation of multicellular spheroids composed of adult rat hepatocytes in dishes with positively charged surfaces and under other nonadherent environments. *Exp. Cell Res.* 186, 227–235. [https://doi.org/10.1016/0014-4827\(90\)90300-Y](https://doi.org/10.1016/0014-4827(90)90300-Y).
- Leszczyński, B., Sojka-Leszczynska, P., Wojtyśiak, D., Wróbel, A., Pędrys, R., 2018. Visualization of porcine eye anatomy by X-ray microtomography. *Exp. Eye Res.* 167, 51–55. <https://doi.org/10.1016/j.exer.2017.11.004>.
- Metscher, B.D., 2009. Micro CT for comparative morphology: simple staining methods allow high-contrast 3D imaging of diverse non-mineralized animal tissues. *BMC Physiol.* 9, 11. <https://doi.org/10.1186/1472-6793-9-11>.
- Milotti, E., Vyshemirsky, V., Sega, M., Chignola, R., 2012. Interplay between distribution of live cells and growth dynamics of solid tumours. *Sci. Rep.* 2, 990. <https://doi.org/10.1038/srep00990>.
- Milotti, E., Vyshemirsky, V., Sega, M., Chignola, R., 2014. Corrigendum: interplay between distribution of live cells and growth dynamics of solid tumours. *Sci. Rep.* 4, 3387. <https://doi.org/10.1038/srep03387>.
- Müller, I., Kulms, D., 2018. A 3D organotypic melanoma spheroid skin model. *J. Vis. Exp.* 135. <https://doi.org/10.3791/57500>. e57500.
- Nofsinger, J.B., Forest, S.E., Simon, J.D., 1999. explanation for the disparity among absorption and action spectra of eumelanin. *J. Phys. Chem. B* 103, 11428–11432. <https://doi.org/10.1021/jp992640y>.
- Pampaloni, F., Ansari, N., Stelzer, E.H.K., 2013. High-resolution deep imaging of live cellular spheroids with light-sheet-based fluorescence microscopy. *Cell Tissue Res.* 352, 161–177. <https://doi.org/10.1007/s00441-013-1589-7>.
- Pitaktong, I., Lui, C., Lowenthal, J., Mattson, G., Jung, W.H., Bai, Y., Yeung, E., Ong, C.S., Chen, Y., Gerecht, S., Hibino, N., 2020. Early vascular cells improve microvascularization within 3D cardiac spheroids. *Tissue Eng. Part C-Methods* 26, 80–90. <https://doi.org/10.1089/ten.tec.2019.0228>.
- Raghavan, S., Ward, M.R., Rowley, K.R., Wold, R.M., Takayama, S., Buckanovich, R.J., Mehta, G., 2015. Formation of stable small cell number three-dimensional ovarian cancer spheroids using hanging drop arrays for preclinical drug sensitivity assays. *Gynecol. Oncol.* 138, 181–189. <https://doi.org/10.1016/j.ygyno.2015.04.014>.
- Rosenhain, S., Magnuska, Z.A., Yamoah, G.G., Al Rawashdeh, W., Kiessling, F., Gremse, F., 2018. A preclinical micro-computed tomography database including 3D whole body organ segmentations. *Sci. Data* 5, 180294. <https://doi.org/10.1038/sdata.2018.294>.
- Shah, S., Lee, H., Park, Y.H., Jeon, E., Chung, H.K., Lee, E.S., Shim, J.H., Kang, K.T., 2019. Three-dimensional angiogenesis assay system using Co-culture spheroids formed by endothelial colony forming cells and mesenchymal stem cells. *J. Vis. Exp.* 151, e60032. <https://doi.org/10.3791/60032>.
- Shi, W., Kwon, J., Huang, Y., Tan, J., Uhl, C.G., He, R., Zhou, C., Liu, Y., 2018. Facile tumor spheroids formation in large quantity with controllable size and high uniformity. *Sci. Rep.* 8, 6837. <https://doi.org/10.1038/s41598-018-25203-3>.
- Society, A.C., 2018. *Key Statistics for Melanoma Skin Cancer*.
- Stepień, E.L., Karimi, H., Leszczyński, B., Szczepanek, M., 2020. Melanoma spheroids as a model for cancer imaging study. *A Phys. Pol. B* 51, 159–163. <https://doi.org/10.5506/APhysPolB.51.159>.
- Torisawa, Y.S., Takagi, A., Nashimoto, Y., Yasukawa, T., Shiku, H., Matsue, T., 2007. A multicellular spheroid array to realize spheroid formation, culture, and viability assay on a chip. *Biomaterials* 28, 559–566. <https://doi.org/10.1016/j.biomaterials.2006.08.054>.
- Wróbel, S., Przybyło, M., Stepień, E., 2019. The clinical trial landscape for melanoma therapies. *J. Clin. Med.* 8, 368. <https://doi.org/10.3390/jcm8030368>.